

# Complexity of calcium signaling in synaptic spines

Kevin M. Franks and Terrence J. Sejnowski\*

## Summary

Long-term potentiation and long-term depression are thought to be cellular mechanisms contributing to learning and memory. Although the physiological phenomena have been well characterized, little consensus of their underlying molecular mechanisms has emerged. One reason for this may be the under-appreciated complexity of the signaling pathways that can arise if key signaling molecules are discretely localized within the synapse. Recent findings suggest an unanticipated degree of structural organization at the synapse, and improved methods in cellular imaging of living tissue have provided much-needed information about the intracellular dynamics of  $\text{Ca}^{2+}$ , thought to be critical for both LTP and LTD. In this review, we briefly summarize some of these developments, and show that a more complete understanding of cellular signaling depends on the successful integration of traditional biochemistry and molecular biology with the spatial and temporal details of synaptic ultrastructure. Biophysically realistic computer simulations can have an important role in bridging these disciplines. *BioEssays* 24:1130–1144, 2002.

© 2002 Wiley Periodicals, Inc.

## Introduction

New techniques such as patch recording, which has made it possible to record currents through single channels, and

multiphoton laser microscopy, which allows visualization of cellular processes with submicron resolution, have revealed a level of complexity in cell signaling that extends spatially to the subcellular level at millisecond time scales. New computational methods have also been developed to model cellular signaling in this regime. Here we review the application of these new modeling techniques to recent experimental data relevant to the modification of the strength of central glutamate synapses.

Most neurons interact through chemical synapses, comprising a pre- and postsynaptic cellular component. The starting point for activating a synapse is an action potential, a regenerative electrical signal, triggered by depolarization, which travels along the axon of the presynaptic cell. When the action potential reaches the synapse, VDCCs in the presynaptic membrane transiently open and, through a series of as yet poorly defined steps, can cause a synaptic vesicle to fuse with the cell membrane, releasing neurotransmitter into the synaptic cleft, a narrow space approximately 20 nm wide, between the two cells. The transmitter then diffuses across the cleft and binds to receptors on the postsynaptic membrane. These receptors are often ion channels, and a conformational change in the receptor as a result of transmitter binding results in a transient opening of its conducting pore. These pores are selective for different ions, whose flux across the membrane generates either an inward or an outward current in the postsynaptic cell, depending on the charge of the ion and the net direction of flux (i.e. into or out of the cell). Different transmitters can therefore result in either an increase (an excitatory synapse that generates an inward current) or a decrease (an inhibitory synapse that generates an outward current) in the probability that the postsynaptic cell will itself generate an action potential and, thus, relay the signal.

Glutamate, the major excitatory transmitter in the brain, binds to at least two distinct types of ionotropic receptors on the postsynaptic membrane; AMPA receptors (AMPA receptors) and NMDA receptors (NMDARs). Although a single EPSC is usually too small to induce an action potential, neurons typically integrate signals from thousands of synapses acting in concert. Thus, small but concerted changes in the efficacy of individual synapses can dramatically alter the behavior of a neuron.<sup>(1)</sup> These changes in synaptic efficacy, termed synaptic plasticity, have been the subject of intense study for the past

Howard Hughes Medical Institute, The Salk Institute, Computational Neurobiology Laboratory, La Jolla and Division of Biology, University of California San Diego.

\*Correspondence to: Terrence J. Sejnowski, Computational Neurobiology Laboratory, The Salk Institute, 10010 North Torrey Pines Road, La Jolla, CA 92037. E-mail: terry@salk.edu

DOI 10.1002/bies.10193

Published online in Wiley InterScience (www.interscience.wiley.com).

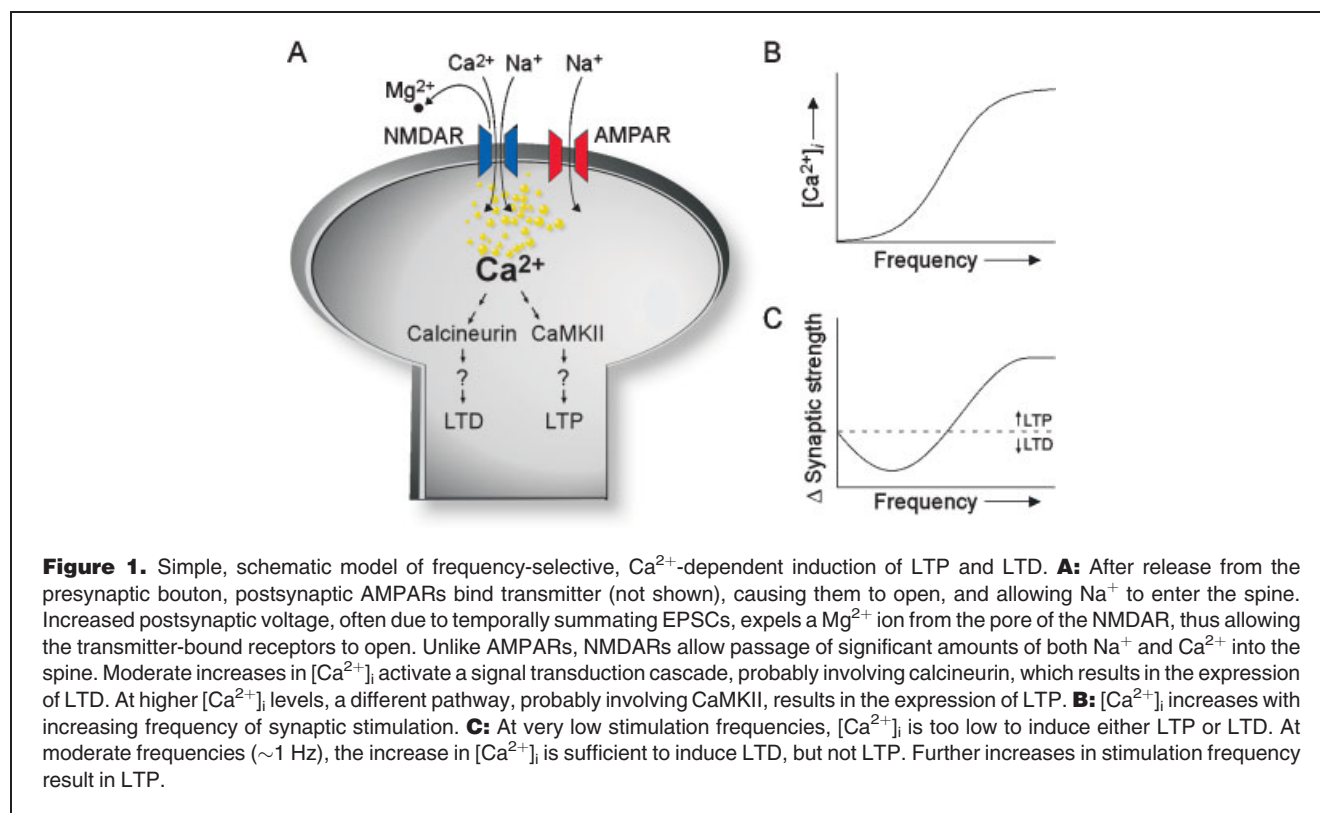
Abbreviations: AMPA,  $\alpha$ -amino-3-hydroxy-5-methyl-isoxazolepropionic acid;  $[\text{Ca}^{2+}]_i$ , free intracellular  $\text{Ca}^{2+}$  concentration; CaM, calmodulin; CaMKII,  $\text{Ca}^{2+}$ /CaM-dependent protein kinase II; CBPs, intracellular  $\text{Ca}^{2+}$ -binding proteins; CREB, cAMP response element binding protein;  $\Delta F/F$ , normalized increase in fluorescence; EPSC, excitatory postsynaptic current; EPSP, excitatory postsynaptic potential; LTD, long-term depression; LTP, long-term potentiation; MAPK, mitogen-activated protein kinase; NMDA, N-methyl-D-aspartate; nNOS, neuronal nitric oxide synthase; PSD, postsynaptic density; STDP, spike-timing dependent plasticity; VDCCs, voltage-dependent  $\text{Ca}^{2+}$  channels.

three decades because changes in synaptic strength could be a cellular correlate of learning and memory.<sup>(2)</sup>

Long-term potentiation was first reported as a persistent increase in synaptic efficacy at synapses of the dentate gyrus in the rabbit hippocampus,<sup>(3)</sup> and has since been found at many other excitatory synapses studied in the mammalian brain. Theorists soon understood the need for a compensatory mechanism to depress synapses,<sup>(4,5)</sup> which was soon reported.<sup>(6–8)</sup> The best-characterized forms of these phenomena are NMDAR-dependent LTP and LTD of excitatory neurons in the CA1 region of the hippocampus. (Henceforth in this review, LTP and LTD refer specifically to the NMDAR-dependent forms of plasticity as principally characterized in pyramidal neurons.) LTP is reliably induced with either a high-frequency train of presynaptic activity or by pairing presynaptic stimulation with postsynaptic depolarization induced by a current injection into the postsynaptic cell, whereas a long train of low-frequency stimulation reliably induces LTD. The manner in which these changes are expressed has been controversial.<sup>(9)</sup> Because the presynaptic neuron may release vesicles with low probability, LTP or LTD could be expressed by either an increase or a decrease in release probability. Alternatively, synaptic efficacy could be increased by an increase in receptor strength or number. It may be that different stimulation conditions favor one or the other of these mechanisms.

### Traditional approach to the induction of LTP and LTD

The induction of LTP and LTD seems to be more straightforward. Glutamate is released from the presynaptic vesicle, diffuses across the synaptic cleft and binds to AMPARs and/or NMDARs, which are often, but not always, colocalized on the postsynaptic membrane.<sup>(10–12)</sup> Doubly liganded AMPARs open, allowing  $\text{Na}^+$  into, and  $\text{K}^+$  out of the cell, causing a small EPSC, and a resulting change in membrane potential, an EPSP. A  $\text{Mg}^{2+}$  ion in the pore of the NMDAR blocks transmission under resting conditions. With strong depolarization, the  $\text{Mg}^{2+}$  ion is expelled from the pore of the channel and the liganded NMDAR opens. The source of depolarization typically includes local summation of EPSPs during a high-frequency burst of presynaptic activity or a direct injection of current into the cell. Open NMDARs, in addition to permitting the influx of  $\text{Na}^+$  and the efflux of  $\text{K}^+$  ions, also allow a significant number of  $\text{Ca}^{2+}$  ions to enter the cell, leading to the suggestion that the NMDAR-mediated increase in intracellular calcium concentration ( $[\text{Ca}^{2+}]_i$ ) in the postsynaptic cell is instrumental in the induction of LTP and LTD. Specifically, a large increase in  $[\text{Ca}^{2+}]_i$ , typically following high frequency stimulation, is thought to induce LTP, whereas a more moderate increase in  $[\text{Ca}^{2+}]_i$ , typically following low frequency stimulation is thought to induce LTD<sup>(13,14)</sup> (Fig. 1).

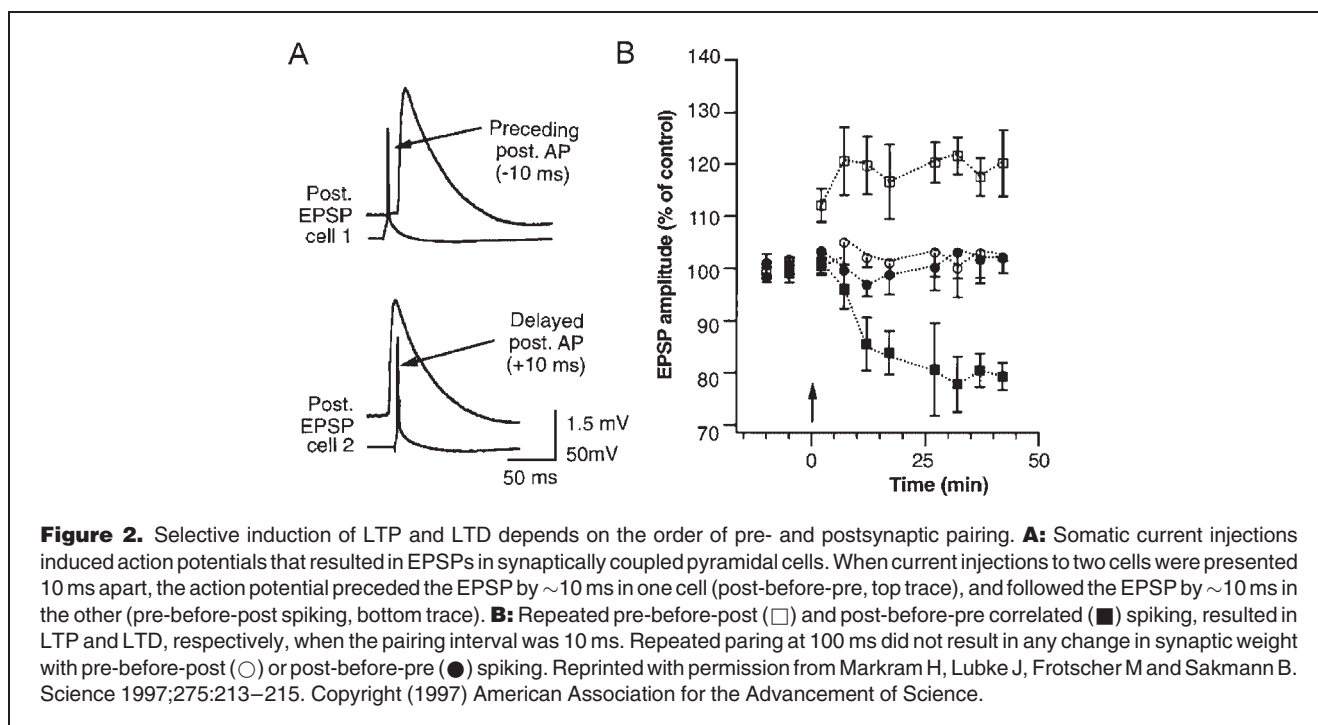


This hypothesis is supported by a number of important findings. First, the addition of  $\text{Ca}^{2+}$  chelators to the postsynaptic cell prevented the induction of LTP<sup>(15,16)</sup> and LTD.<sup>(17)</sup> Second, induction of LTP and LTD was shown to depend on the activation of  $\text{Ca}^{2+}$ -dependent kinases (CaMKII)<sup>(18,19)</sup> and phosphatases (Calcineurin),<sup>(20,21)</sup> respectively. Third, decreasing the influx of  $\text{Ca}^{2+}$  through NMDARs with non-saturating concentrations of a NMDAR antagonist induces LTD with an otherwise LTP-inducing stimulation protocol.<sup>(22,23)</sup> Fourth, increasing extracellular calcium concentration, and thus  $\text{Ca}^{2+}$  influx, can induce a mild LTP with low-frequency (i.e. LTD-inducing) stimulation,<sup>(24)</sup> and decreasing extracellular calcium concentration can induce LTD with high-frequency (i.e. LTP-inducing) stimulation.<sup>(17)</sup> Furthermore, genetic manipulation of the NMDAR subunit composition resulting in an increase in the amount of  $\text{Ca}^{2+}$  entering the cell results in LTP induction at lower stimulation frequencies.<sup>(25)</sup> Fifth, direct manipulation of postsynaptic  $\text{Ca}^{2+}$  levels using diffuse photolytic uncaging of chelated  $\text{Ca}^{2+}$  is sufficient to induce both LTP and LTD.<sup>(16,26–28)</sup> Specifically, *large* ( $\sim 10 \mu\text{M}$ ), *brief* ( $\sim 3$  sec) increases in  $[\text{Ca}^{2+}]_i$  reliably induce LTP, whereas a *modest* ( $\sim 0.7 \mu\text{M}$ ), *long* ( $\sim 60$  sec) increases in  $[\text{Ca}^{2+}]_i$  reliably induce LTD.<sup>(28)</sup>

### Spike-timing-dependent plasticity

The temporal order of pre- and postsynaptic activation may also be important for the selective induction of LTP and LTD.<sup>(7,29)</sup> With the finding that an action potential, or spike,

induced by a current injection into the soma, not only travels down the axon but also propagates back through the dendrites,<sup>(30)</sup> the timing of the presynaptic input (the release of glutamate) and the postsynaptic output (the spike) can be controlled with millisecond precision. A fascinating picture has since emerged. LTP is reliably induced when the presynaptic cell is repeatedly made to fire an action potential shortly before the postsynaptic cell (pre-before-post), and LTD is induced when the order is reversed (post-before-pre; Fig. 2). This finding is robust and has been found in neurons from the hippocampus using acute,<sup>(23)</sup> organotypic slices,<sup>(31)</sup> or dissociated cell culture,<sup>(32)</sup> and in layers V<sup>(33,34)</sup> and II/III<sup>(35)</sup> of the cerebral cortex, as well as in vivo preparations using cat<sup>(36,37)</sup> and *Xenopus*<sup>(38)</sup> visual systems. The temporal window permissive for LTP induction is 10–20 ms (milliseconds) whereas the window in which the presynaptic spike can follow the postsynaptic spike in order to induce LTD ranges from 20 to 100 ms in different preparations. This form of synaptic plasticity has been termed STDP. Induction of STDP is dependent on NMDAR and intracellular  $\text{Ca}^{2+}$ , and partial blockade of NMDARs can induce LTD with a positively correlated pairing protocol.<sup>(23)</sup> In fact, pairings of pre-before-post result in a superlinear increase in  $[\text{Ca}^{2+}]_i$ ,<sup>(39–43)</sup> and post-before-pre pairings result in a sublinear increase in  $[\text{Ca}^{2+}]_i$ .<sup>(41)</sup> Thus, although the exact mechanisms remain unknown, it is likely that this form of synaptic plasticity shares many properties with the traditional, frequency-dependent forms of LTP and LTD.



### Ca<sup>2+</sup> in dendritic spines

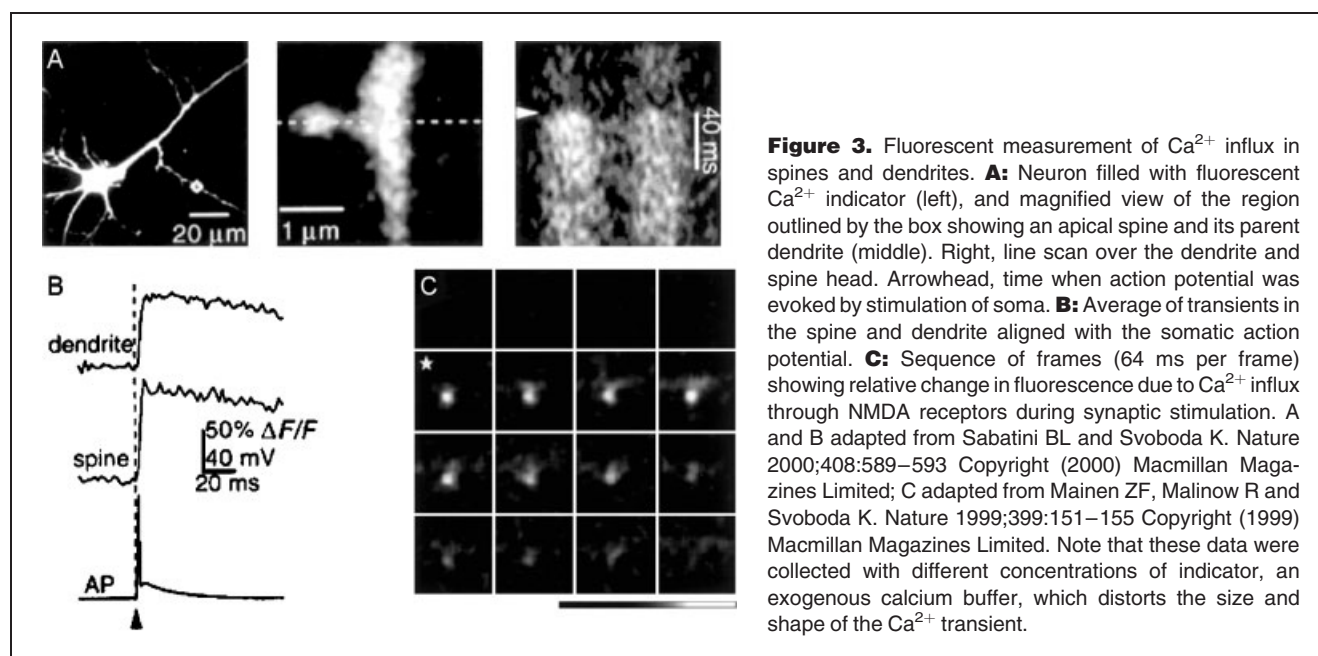
The majority of excitatory synapses between neurons in the mammalian brain are made onto dendritic spines, small protrusions from the shaft of the dendrite, whose primary function may be to compartmentalize calcium. In the past decade, important developments in multiphoton imaging<sup>(44)</sup> and calcium-sensitive fluorescent dyes<sup>(45)</sup> have allowed researchers to probe the dynamics of intracellular Ca<sup>2+</sup> at temporal and spatial resolutions of  $\sim 1$  ms and  $\sim 1$   $\mu$ m, respectively: the spatial resolution of a single spine, and at the temporal resolution of synaptic currents. Together, these have made possible the measurement of Ca<sup>2+</sup> influx through either VDCCs during an action potential (Fig. 3A,B) or NMDARs during an EPSP (Fig. 3C). Recent reviews summarize the wealth of information that has been gleaned from these experiments.<sup>(46,47)</sup> In particular, Svoboda and colleagues<sup>(43,48,49)</sup> have provided much needed quantitative information about Ca<sup>2+</sup> dynamics in dendritic spines. The fundamental assumption underlying these experiments is that the spine can be treated as a single compartment. With this caveat, important principles can be determined using the amplitude and decay of the fluorescent transients elicited with different concentrations of fluorescent indicator, and extrapolating to conditions in the unperturbed spine (i.e. with no exogenous buffer). Under these conditions, about 80% of the Ca<sup>2+</sup> ions that enter the cell are rapidly buffered by CBPs. Single, unpaired action potentials or EPSPs result in sharp increases in [Ca<sup>2+</sup>]<sub>i</sub> which both peak at  $\sim 1$   $\mu$ M. The action-potential-induced increase in [Ca<sup>2+</sup>]<sub>i</sub> decays within 20 ms. Although the NMDAR-mediated synaptically evoked increase

in [Ca<sup>2+</sup>]<sub>i</sub> is broader because of the slow kinetics of the NMDARs ( $\tau \sim 100$  ms), the kinetics of Ca<sup>2+</sup> extrusion following an EPSP are similar to those following an action potential. Importantly, presentation of the EPSP just before the action potential (i.e. a pre-before-post) results in a large increase in [Ca<sup>2+</sup>]<sub>i</sub> which peaked at  $\sim 10$   $\mu$ M, and decays at rates similar to the unpaired stimuli.<sup>(43)</sup>

### Can frequency-dependent plasticity and STDP be reconciled?

LTP and LTD have been reliably induced with pre-before-post and post-before-pre pairings presented at frequencies as low as 0.133 Hz.<sup>(35)</sup> Although 50–100 pairing sweeps were presented in these experiments, imaging studies suggest that [Ca<sup>2+</sup>]<sub>i</sub> returns to resting levels within  $<100$  ms. Thus, although the peak [Ca<sup>2+</sup>]<sub>i</sub> amplitudes for pre-before-post and post-before-pre pairing protocols are consistent with the [Ca<sup>2+</sup>]<sub>i</sub> levels shown to be necessary for the selective induction of LTP and LTD by uncaging, the time courses of the calcium elevations are 10–100 times too short.<sup>(26)</sup> Thus, there is an apparent contradiction. Pairing protocols that are NMDAR-dependent and almost certainly Ca<sup>2+</sup>-dependent are able to selectively induce LTP or LTD, but, according to uncaging experiments, the elevations in intracellular calcium that these protocols induce are too brief to reliably induce either. The overlooked assumption may be the treatment of the spine as a single compartment.

Caged Ca<sup>2+</sup> was released using a diffuse light source that can be assumed to have increased intracellular calcium levels in the spine homogeneously.<sup>(16,27,28)</sup> The spine can



therefore be treated as a single compartment with respect to  $[Ca^{2+}]_i$  under these conditions; ignoring gradients induced by the spatial localization of  $Ca^{2+}$  pumps and exchangers on membrane surfaces. However, the spine cannot be considered a single calcium compartment for normal physiological stimuli.  $Ca^{2+}$  entry, particularly through NMDARs, which are localized on the synaptic face of the spine, will create a concentration gradient across the spine, with high concentrations, as high as hundreds of  $\mu M$ , near the mouth of the channel.<sup>(50)</sup>

The amount of time  $[Ca^{2+}]_i$  needs to be elevated to induce either LTP or LTD is a function of the probability of  $Ca^{2+}$  ions encountering and activating sufficient numbers of specific target proteins. For uncaging experiments, this can take a long time given the relatively small number of free  $Ca^{2+}$  ions (see below), particularly if these proteins are neither rapidly diffusing nor homogeneously distributed. However, if these proteins are concentrated very near the NMDARs, the probability of their activation can be orders of magnitude greater than if the same number of free  $Ca^{2+}$  ions are uniformly distributed through the spine. Thus, we suggest that the differences in the amount of time  $Ca^{2+}$  levels need to be elevated to induce long-lasting changes in synapse strength following either  $Ca^{2+}$  uncaging or physiological stimuli is due to emergent signaling properties of  $Ca^{2+}$ -dependent effector proteins given their spatial relationship with sites of  $Ca^{2+}$  entry into the spine. This hypothesis requires at least two assumptions: first, that  $Ca^{2+}$ -dependent signaling molecules are able to respond to micro- or even nanodomain increases in  $[Ca^{2+}]_i$  and, second, that such spatial organization of protein-effectors exist at glutamatergic synapses. Recent evidence, however, suggests that both these assumptions are valid.

### Nanodomain activation of $Ca^{2+}$ -dependent reactions

The first assumption is strongly supported by recent experiments investigating the initiation of  $Ca^{2+}$ -dependent gene transcription. Under physiological conditions, activation of calcium-dependent signal transduction pathways can depend on the mode of entry of  $Ca^{2+}$  into the cell. For example, the calcium-dependent phosphorylation of CREB, which drives the expression of a number of genes that regulate neuronal plasticity and survival,<sup>(51)</sup> depends specifically on  $Ca^{2+}$  influx through L-type VDCCs.<sup>(52)</sup> A recent study has shown that this specificity arises because CaM is tethered to the cytoplasmic tail of the channel, where it is activated by  $Ca^{2+}$  ions entering the cell when the channel opens. Activated CaM then binds to an IQ domain near the COOH terminal of the channel, and activates the MAPK pathway that results in CREB phosphorylation.<sup>(53)</sup> Thus, the L-type channel is not merely a means for increasing overall calcium levels. It also serves as an organizational scaffold

on which downstream calcium-dependent effector proteins are optimally positioned to bind  $Ca^{2+}$  ions entering through the pore of the channel. Once activated, CaM binds a different site of the same protein, and the signal transduction cascade is initiated. This elegant example is not unique. Very local  $Ca^{2+}$ -dependent signaling has been demonstrated at numerous other sites, including  $Ca^{2+}$  entering through NMDARs.<sup>(54,55)</sup>

### PSD organization

Observed by early microscopists as a thickening of the postsynaptic membrane, the postsynaptic density (PSD) is a dense protein complex extending approximately 40 nm into the cytosol. Both AMPA and NMDA receptors are anchored in the PSD by different signaling and scaffolding proteins. Thus, the proteins of the PSD are the first targets for  $Ca^{2+}$  ions entering the spine through NMDARs. There are 30–100 proteins directly bound to, or associated with, the NMDA receptor, forming a large NMDA receptor complex<sup>(56–58)</sup> (Fig. 4). A characterization of the proteins comprising the PSD is beyond the scope of this paper, and has been recently reviewed.<sup>(59,60)</sup> Suffice it to say that many proteins thought essential for the induction and/or expression of both LTP and LTD form part of the PSD complex,<sup>(57)</sup> including CaMKII,<sup>(19,61)</sup> protein phosphatase I,<sup>(20)</sup> calcineurin,<sup>(59,60)</sup> nNOS<sup>(62)</sup> and MAPK.<sup>(63)</sup>

In addition to signaling proteins, the PSD also contains scaffolding proteins. One such protein is PSD-95 (also called SAP-90), first isolated by Kennedy and colleagues.<sup>(64)</sup> Although PSD-95 has no detectable enzymatic activity, it acts as an adaptor molecule through protein–protein interactions mediated through discrete domains; three amino-terminal PDZ domains are followed by an SH3 domain and a guanylate kinase-like domain.<sup>(65)</sup> The three PDZ domains each have slightly different binding specificities and can interact with a variety of different proteins. Because the first and second PDZ domains bind tightly to the NMDAR,<sup>(66,67)</sup> PSD-95 therefore serves as a scaffold between the NMDAR and other signaling proteins of the PSD.

Although PSD-95 appears to be involved in the synaptic targeting and clustering of NMDARs,<sup>(66,68,69)</sup> a mouse lacking functional PSD-95 (a stop codon in the third PDZ domain, leaving the first two intact) showed that NMDA receptors were appropriately clustered in the PSD and generated normal synaptic responses.<sup>(70)</sup> However, the properties of synaptic plasticity in these mice were unusual. Using standard induction procedures (including both high frequency stimulation trains and pre-before-post pairing), LTP levels were significantly greater than normal. Moreover, low frequency stimulation trains that should have produced LTD resulted instead in LTP (Fig. 4C).

How do these data fit with the hypothesis that intracellular calcium levels selectively induce LTP and LTD? Note that

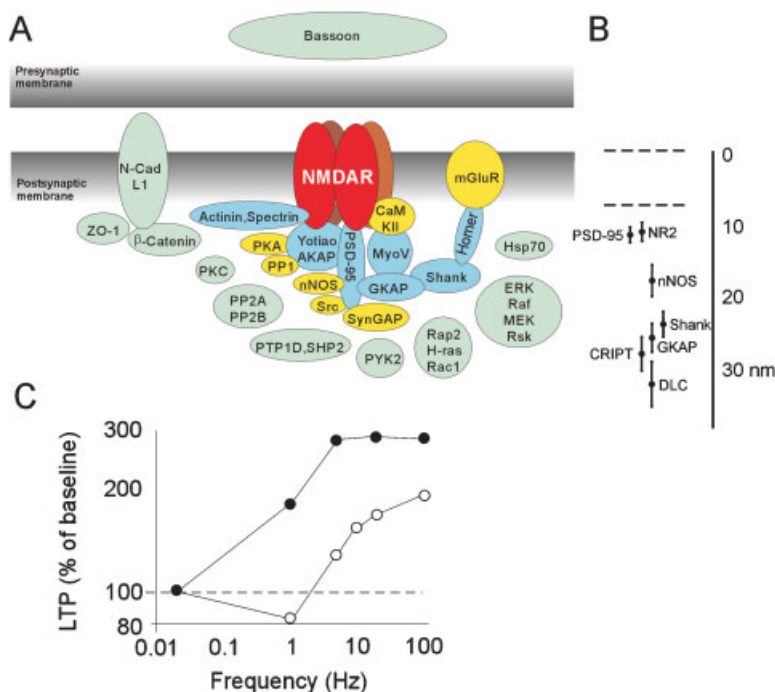


**Figure 4.** Functional organization of the postsynaptic density. **A:** Schematic depiction showing components identified as being associated with the NMDA receptor signaling complex from a recent proteomics study<sup>(57)</sup> (light blue), together with previously identified scaffolding (dark blue) and signaling (yellow) proteins. **B:** Anatomical measurement of postsynaptic localization of signaling proteins using quantitative electron microscopy techniques. **C:** Expression of LTD switches to LTP with increasing stimulation frequency in CA1 synapses of normal mice (○). By contrast, PSD-95 knock-out mice express a robust LTP at all stimulation frequencies (●). A adapted from Sheng M and Lee SH. *Nat Neurosci* 2000;3:633–635 Copyright (2001) by the Society for Neuroscience. B adapted with permission from Valtschanoff JG and Weinberg RJ. *J Neurosci* 2001;21:1211–1217 Copyright (2001) by the Society for Neuroscience. C adapted from Migaud M, Charlesworth P, Dempster M, Webster LC, Watabe AM, Makhinson M, He Y, Ramsay MF, Morris RG, Morrison JH, O'Dell TJ and Grant SG. *Nature* 1998;396:433–439 Copyright (1998) Macmillan Magazines Limited.

PSD-95 does not affect NMDA receptor currents, so the calcium levels in mutant and wild-type mice were presumably similar. Perhaps disruption of the NMDA receptor complex by knocking out PSD-95 displaced a low-affinity  $\text{Ca}^{2+}$ -dependent signaling protein responsible for the induction of LTD away from the site of  $\text{Ca}^{2+}$  entry (the NMDAR), preventing the induction of LTD. A model for the bidirectional control of synaptic strength involves competing actions of kinase (LTP) and phosphatase (LTD) activity.<sup>(71,72)</sup> Thus a decrease in phosphatase activity could explain both the lack of LTD and the enhanced LTP seen in these mice.

These apparent inconsistencies suggest that identifying and characterizing the participating cellular effectors is only the first step in achieving a full understanding of the steps underlying the induction of LTP and LTD,<sup>(73)</sup> and intracellular signal processing in general. At least equally important is the task of understanding how these proteins are organized in the postsynaptic membrane to produce normal synaptic function. This will require analysis of the spatial dependence and,

importantly, the interdependence, of the appropriate signaling proteins.

#### Novel approaches using computer modeling

Biophysically realistic computer simulations offer a powerful tool with which to explore cellular signaling at fine spatial and temporal scales. The simplest approach to modeling synaptic signaling involves solving a set of differential equations for a single, well-mixed compartment. This method has been successfully used in fields like physical chemistry and traditional biochemistry, where the well-mixed approximation is satisfied. Unfortunately, these models ignore the structural detail of the synapse, and often fall short of providing a satisfying, biologically accurate explanation of the phenomena being modeled.

To include spatial information, two different approaches to kinetic modeling have been proposed. The “finite element” approach (FE) divides three-dimensional space into a regular grid of contiguous subcompartments, or voxels. It assumes

well-mixed conditions within each voxel, and uses differential equations to compute fluxes between, and reactions within each voxel. This approach is well suited to large, simple volumes with large numbers of a few types of molecules, such as a test-tube. Complex cellular structures, however, require the grid be very fine and irregular in shape, making this approach both computationally expensive and difficult to program. Furthermore, as voxel size decreases, the product of the voxel volume and reactant concentration can yield fractional numbers of molecules, and multiple reaction partners and complex signaling pathways increase the dimensionality of the differential equations, further increasing the computational load.

Although mass-action equations still predict correct average concentrations, the discrete and stochastic nature of signaling, which becomes important when the number of molecules is small, is ignored using the FE approach. This is especially true for calcium-dependent signaling. For example, a 50 nm resting  $[Ca^{2+}]_i$  in a dendritic spine ( $0.1 \mu m^3$ ) entails an average of only three free  $Ca^{2+}$  ions. Similarly, a  $[Ca^{2+}]_i$  of 1  $\mu M$ , a high level at which calcium is able to induce biochemical changes in the spine, still only corresponds to  $\sim 60$  free  $Ca^{2+}$  ions. If a spine, modeled as a cube,  $0.5 \mu m$  on a side, were coarsely divided into a  $10 \times 10 \times 10$  grid, the average number of  $Ca^{2+}$  ions in each voxel, would be 0.06, an unphysical number. Thus, the FE method will fail to accurately describe the biochemistry of synaptic signaling because these methods only provide averaged data, ignoring the stochastic nature of signaling, and because a biophysically realistic simulation, complete with an accurate three-dimensional structure of the system, is likely to be too difficult to program and too computationally expensive.

The other approach uses Monte Carlo methods, where random numbers and probabilities are used to simulate individual cases of the system's behavior (see Box 1). MCell is a highly optimized Monte Carlo simulation program that can be used to address complex biological problems (<http://www.mcell.cnl.salk.edu>).<sup>(74,75)</sup> Unlike FE, diffusion of individual ligand molecules are simulated using a Brownian dynamics random walk algorithm, and bulk solution rate constants are converted into Monte Carlo probabilities so that the diffusing ligands can undergo stochastic chemical interactions with individual binding sites such as receptor proteins, enzymes, transporters, etc (see Box 2).

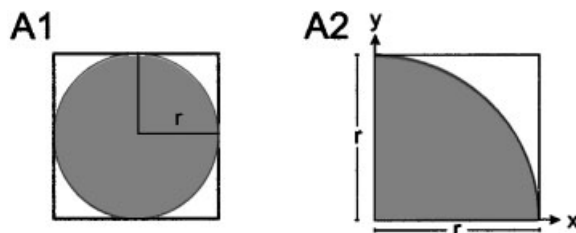
The development of MCell started as a project in the laboratory of the late Miriam Salpeter at Cornell University to accurately simulate activation of postsynaptic receptors at the neuromuscular junction.<sup>(76–78)</sup> More recently, these algorithms have also been used to study synaptic activation at central synapses.<sup>(79–81)</sup> We have used MCell to simulate intracellular  $Ca^{2+}$  dynamics in dendritic spines, with a long-term goal of understanding the critical time-window underlying STDP. This will require implementation in a structure with

realistic geometry, knowledge of the number and location of all the critical proteins, the dynamics of  $Ca^{2+}$  at single synapses, and their interactions. This is an on-going project requiring extensive collaboration between groups with widely different sets of expertise. The first stage of this task, the simulation of  $Ca^{2+}$  dynamics in an idealized dendritic spine, and its interaction with a small number of CBPs, is summarized here. The model involves  $Ca^{2+}$  influx,  $Ca^{2+}$  efflux, intracellular buffering and the activation of intracellular CaM.  $Ca^{2+}$  can enter the spine through VDCCs during an action potential or through NMDARs following glutamate release. Once inside the spine,  $Ca^{2+}$  is extruded via pumps on the spine apparatus, an extension of the dendritic endoplasmic reticulum, and pumps and exchangers on the cell membrane, and CBPs, distributed throughout the cytoplasm, bind and buffer  $[Ca^{2+}]_i$ . In addition to quantitative simulation of complex signal transduction cascades, this type of model can also serve another, extremely powerful function; because the spatial location of each molecule is tracked, the simulated intracellular environment can be graphically rendered, providing a conceptual view of the structure and dynamics of the system. To illustrate this, we have modeled and visualized  $Ca^{2+}$  influx following either an action potential or EPSP.

### Action potential-induced $Ca^{2+}$ influx

In a simulation of an action potential evoked by somatic current injection using the NEURON<sup>(82)</sup> simulation environment, the action potential propagated back through the dendrites to the spine resulting in a brief depolarization (Fig. 5A). Spines typically contained four or five VDCCs, which open with a probability of  $\sim 0.5$  at the peak of the action potential. The voltage time course at the spine was used as input to MCell. On this trial, the spine had three VDCCs, two of which opened briefly at the peak of the action potential (Fig. 5B), resulting in a large  $Ca^{2+}$  influx. Inside the cytoplasm,  $Ca^{2+}$  could be extruded via membrane pumps, or buffered by binding endogenous CBPs (200  $\mu M$ ;  $K_D$ , 2  $\mu M$ ;  $K_{for}$ ,  $10^{7-9} M^{-1} s^{-1}$ ) or exogenous, high-affinity fluorescent  $Ca^{2+}$  indicator (100  $\mu M$ ;  $K_D$ , 233 nM;  $K_{for}$ ,  $0.6 \times 10^9 M^{-1} s^{-1}$ ). The amount of bound indicator, normalized by resting levels ( $\Delta F/F$ ) could be measured and compared to experimental results to test and constrain the model (Fig. 5C; compare with Fig. 3B). Importantly, the model also allows direct measurement of free  $Ca^{2+}$  levels. Here, we show  $[Ca^{2+}]_i$  in the presence of indicator (Fig. 5D). These data are similar to experimental measures, although  $[Ca^{2+}]_i$  in the model had a very large, rapidly decaying component not predicted by the fluorescent signal.

This large  $Ca^{2+}$  spike was due to local saturation of buffer in the cytoplasm surrounding open VDCCs, which can be better understood by visualizing the model output; shown here as four *snapshots* at 4.8 ms, 5.9 ms, 10 ms and 100 ms after the somatic current injection. For each of these panels, the observer is inside the spine. A closed VDCC (translucent, blue



### BOX 1 MONTE CARLO METHODS

Monte Carlo methods provide approximate solutions to a variety of mathematical problems by performing statistical sampling experiments. Although there exist a number of undeveloped earlier instances of their use, systematic development of Monte Carlo methods date from the use of random sampling to simulate the flight paths of neutrons by Stanislaw Ulam and John Von Neumann during the Manhattan Project. Because of the similarity of statistical simulation to games of chance, Nicholas Metropolis, a colleague of Ulam and Von Neumann at Los Alamos, coined the term after the capital of the principality of Monaco, famous for its casinos.

Monte Carlo methods are based on the concept that any part of a function to be integrated over may be thought of as a normalized probability distribution over the region of integration. A simple illustrative example is a geometric Monte Carlo experiment that calculates  $\pi$  using a “hit or miss integration”. Consider a circle with radius  $r$  circumscribed by a square (Fig. A1). Note that because of its geometrical symmetry, the problem can be equivalently considered in terms of a single quadrant (Fig. A2).

Given that

$$\text{Area}_{\text{square}} = r^2$$

and

$$\text{Area}_{\text{quadrant}} = \frac{1}{4}\pi r^2$$

then

$$\pi = 4 \frac{\text{Area}_{\text{quadrant}}}{\text{Area}_{\text{square}}}$$

Now, imagine randomly throwing a large number darts at Fig A2. The essence of the Monte Carlo method is that, as the number of darts increases, the fraction of darts within the quadrant (red shaded area), scaled by 4, will approach the value of  $\pi$ . Implementation of this experiment on a computer is extremely simple, but needs a good random number generator that generates numbers from 0 to 1 from a uniform distribution. Thus, a simple code to perform this experiment might look like:

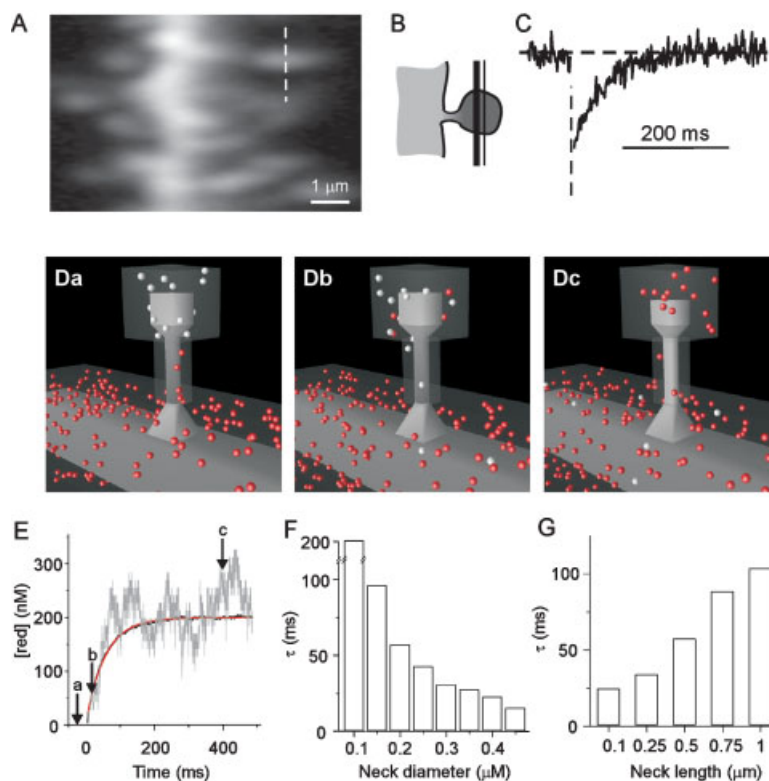
```

r = 1
total_throws = large_number
throw_number = 0
hits = 0
while throw_number ≤ total_throws {
  x = (random_number)
  y = (random_number)
  distance = √{x2 + y2}
  if distance ≤ 1 {
    hits = hits + 1
  }
  throw_number = throw_number + 1
}
π = 4 * hits / total_throws

```

Note that the accuracy of this approximation depends on the number of random trials. It can be proven that the estimate converges to the correct value of  $\pi$  as the number of trials increases to infinity.

By filling cells with fluorescein dextran and using two-photon scanning laser microscopy, Svoboda and colleagues were able to image and photobleach dendritic spines on pyramidal neurons from hippocampal slices. The time-course of the recovery from of spine fluorescence provided a direct measure of the diffusional coupling between the spine and its parent dendrite.<sup>(89)</sup> We have simulated this experiment using MCell to demonstrate random-walk diffusion and the inherent stochasticity of the program. We separated two sets of spheres (white and red) into the spine and parent dendrite, respectively, and then allowed the spheres to diffuse freely between the two structures, which were connected by a narrow spine neck. Although individual trials were noisy, the averaged result was indistinguishable from an exponential decay function, as expected. These simulations demonstrate the dependence on the diffusional coupling rate on the diameter and length of the spine neck (see also Svoboda et al., 1996, Ref 89, Majewska et al., 2000 Ref. 90).

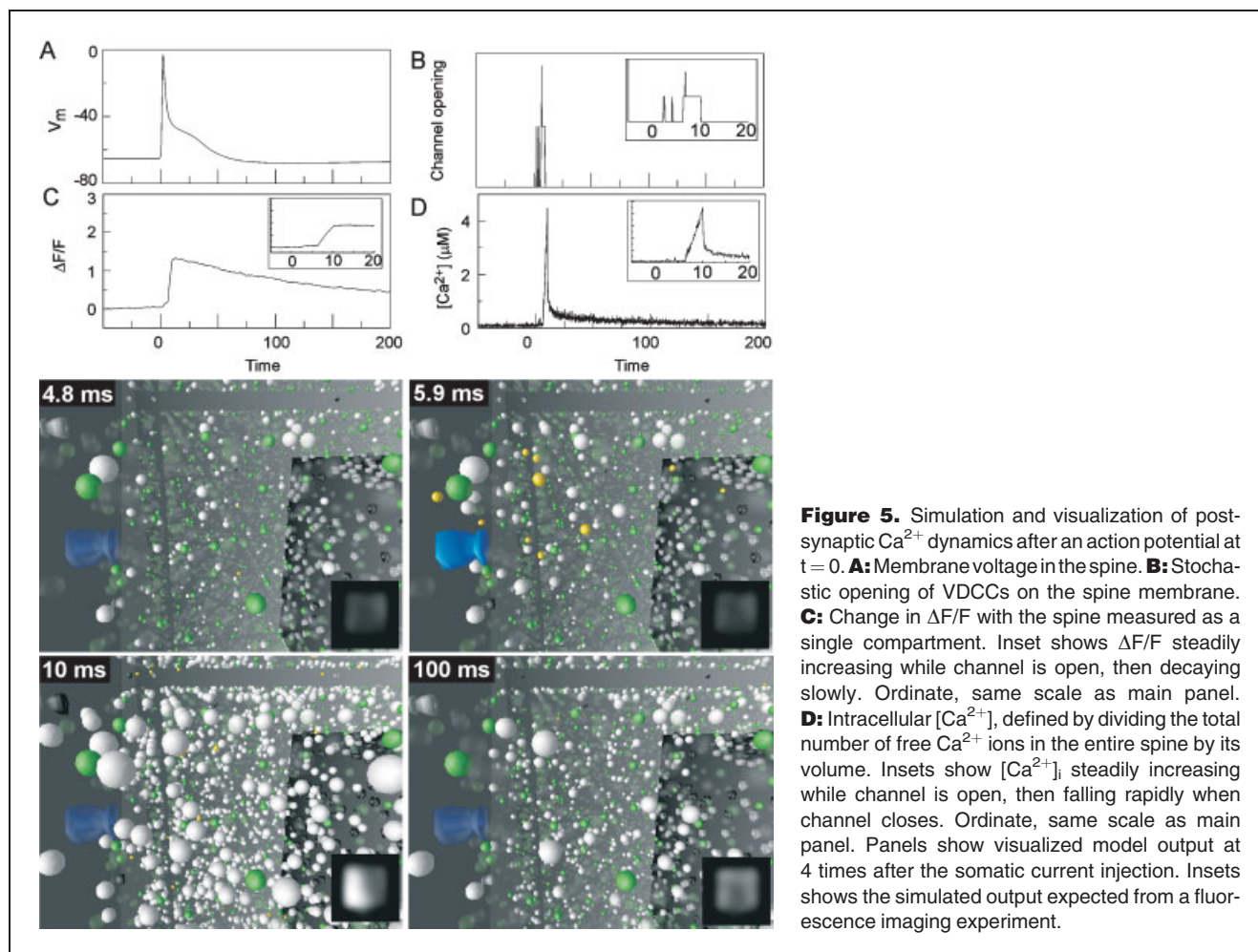


#### BOX 2 RANDOM-WALK DIFFUSION AND STOCHASTICITY IN MCELL

Comparison of recovery from photobleaching in a spine with a Monte Carlo simulation. (A) Fluorescent image of a CA1 pyramidal cell dendrite filled with fluorescein dextran. (B) Schematic depicting experimental protocol. Thin line, locations of fluorescence measurement; thick line, location of photobleaching. Dashed line in (A) corresponds to imaging and bleaching lines in (B). (C) Time course of fluorescence in the spine before and after photobleaching (average of 7 scans). (D) Images and (E) time course of red sphere concentration in the spine from MCell simulations. Individual panels in (D) correspond to times indicated by arrows in (E). Gray trace shows a single trial; black trace, average of 50 trials; red trace, exponential fit to average with  $\tau = 56$  ms. Dependence of  $\tau$  on spine neck (F) diameter and (G) length. A–C adapted with permission from Svoboda K, Tank DW and Denk W. *Science* 1996;272:716–719. Copyright (1996) American Association for the Advancement of Science.

structure) is seen protruding through the cell membrane on the right, and the spine apparatus, an extension of dendritic smooth endoplasmic reticulum, seen as a darkened, cubic structure to the left. Exogenous indicator molecules (green)

and endogenous CBPs (white) are depicted as spheres distributed throughout the cytoplasm, and may be either  $\text{Ca}^{2+}$ -bound (opaque) or  $\text{Ca}^{2+}$ -free (translucent). For comparison with imaging experiments, the spine volume was also



divided into voxels 25 nm on a side, in which the number of bound and unbound indicator molecules inside each voxel were counted and converted to a gray-scale value. Each voxel was then blurred to 250 nm resolution, and rendered as a simulated fluorescent image.

At rest, a small fraction of the indicator and CBPs were bound (4.8 ms). When the channel opened (opaque blue structure),  $\text{Ca}^{2+}$  ions (small yellow spheres) entered the spine, and were rapidly bound by indicator or CBPs close to the mouth of the channel. Immediately after entering the cell,  $\text{Ca}^{2+}$  remained free, thus increasing  $[\text{Ca}^{2+}]_i$  but not depicted as an increase in  $\Delta F/F$  until a significant number of indicator molecules were bound (5.9 ms).  $\text{Ca}^{2+}$  ions continued to enter through the open channel, describing an ever-larger volume of buffer saturation about the mouth of the channel, thus increasing the volume in which  $\text{Ca}^{2+}$  remains free and leading to the large amplitude of the  $[\text{Ca}^{2+}]_i$  spike. When the VDCC closed,  $[\text{Ca}^{2+}]_i$  dropped precipitously as free  $\text{Ca}^{2+}$  rapidly diffused out of the volume of saturated buffer around the channel mouth. By this time, a significant amount of indicator

around the channel was bound, resulting in a measurable fluorescent signal. After 100 ms  $[\text{Ca}^{2+}]_i$  had returned to resting levels as  $\text{Ca}^{2+}$  ions had either been extruded or buffered. However, a significant fraction of the high-affinity indicator was still  $\text{Ca}^{2+}$ -bound, yielding the slowly decaying  $\Delta F/F$  signal.

### EPSP-induced $\text{Ca}^{2+}$ influx

We next examined intracellular  $\text{Ca}^{2+}$  dynamics evoked by synaptic stimulation. Imaging experiments suggest that  $\text{Ca}^{2+}$  influx through NMDARs results in  $\text{Ca}^{2+}$  transients with similar amplitudes and slower kinetics, as compared with  $\text{Ca}^{2+}$  transients evoked by action potentials. Vesicular release of glutamate resulted in an average of 3 of 20 NMDARs opening at peak, and closed with a decay time constant of  $\sim 100$  ms;<sup>(81)</sup> however most of the receptors were unable to conduct because of the  $\text{Mg}^{2+}$  block. The small voltage deflection associated with a single, subthreshold EPSP (Fig. 6A) resulted in a small increase fraction of unblocked receptors, although NMDARs continued to rapidly flicker open (mean open-time,  $\sim 100$   $\mu\text{s}$ ) with low probability at resting potentials, as long as

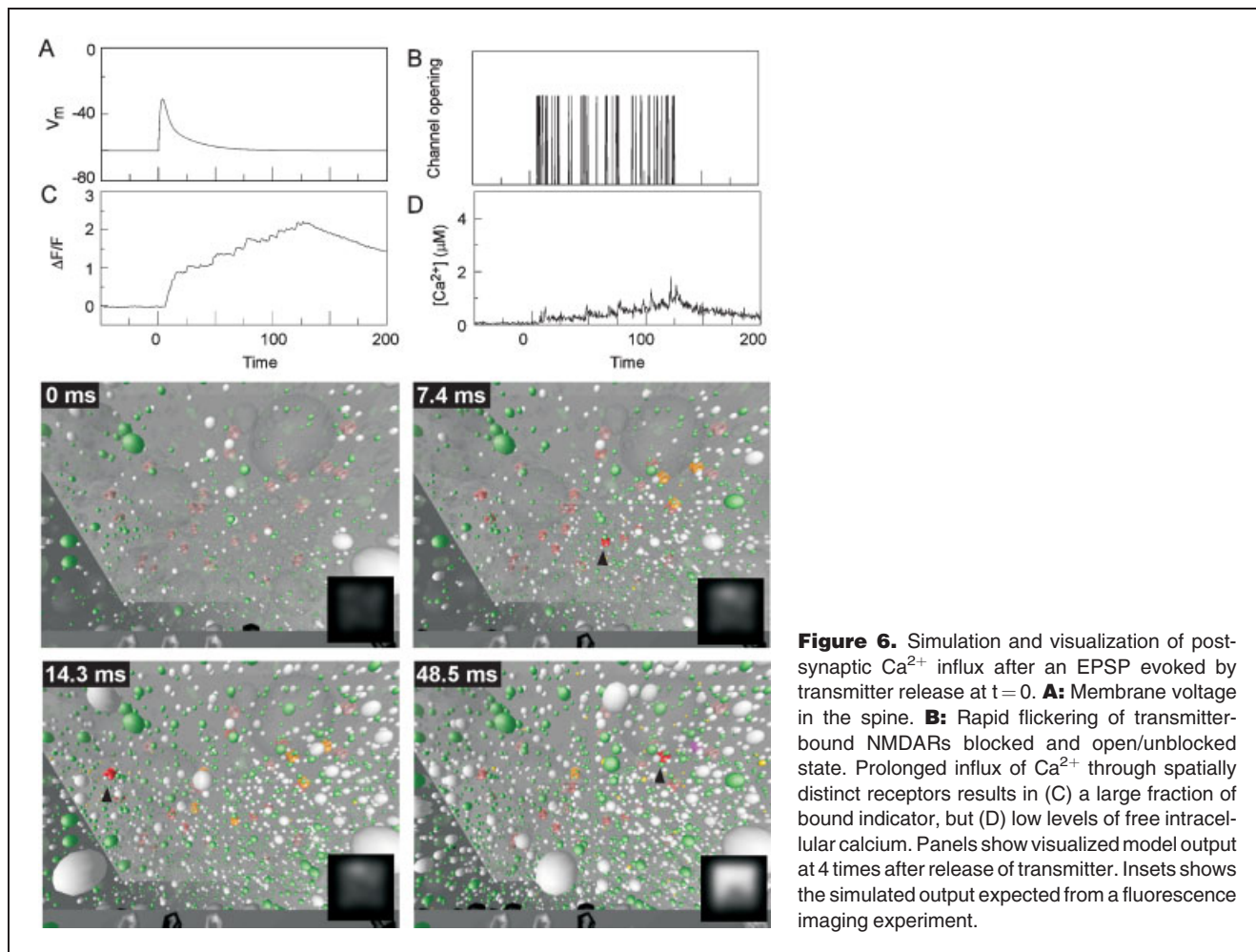


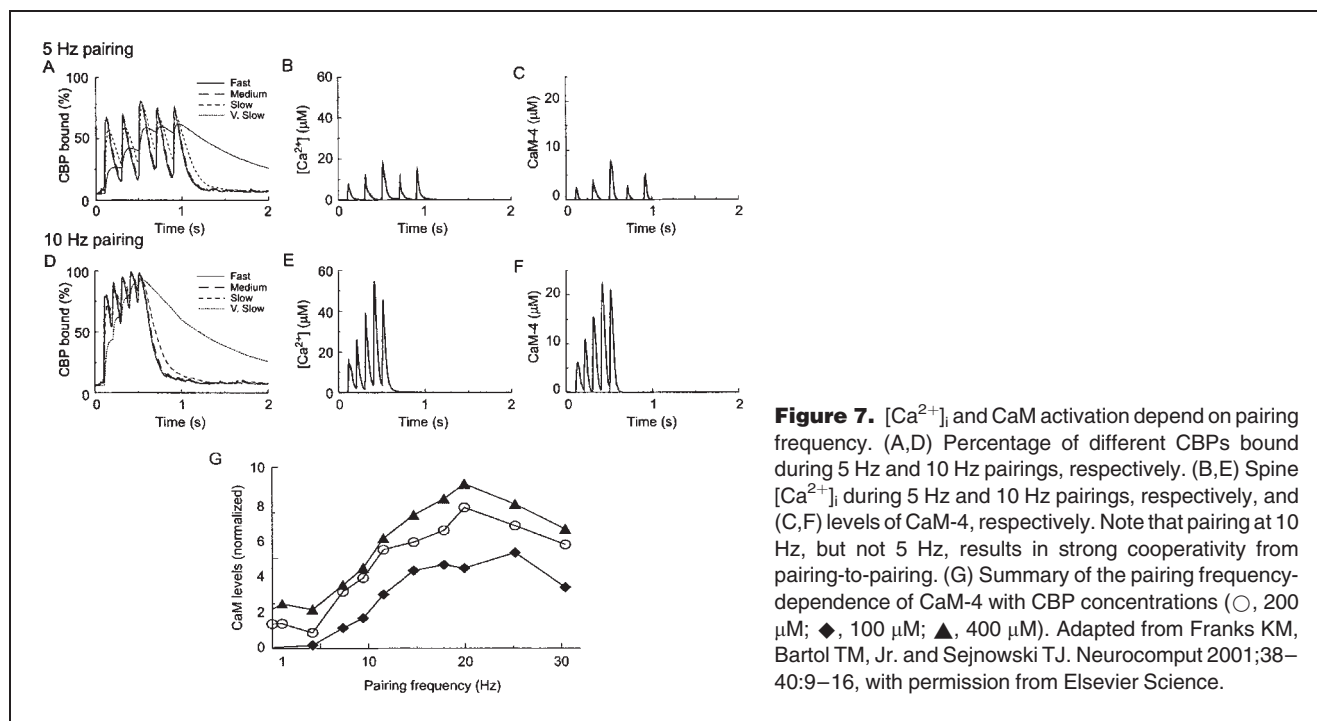
**Figure 6.** Simulation and visualization of post-synaptic  $\text{Ca}^{2+}$  influx after an EPSP evoked by transmitter release at  $t = 0$ . **A:** Membrane voltage in the spine. **B:** Rapid flickering of transmitter-bound NMDARs blocked and open/unblocked state. Prolonged influx of  $\text{Ca}^{2+}$  through spatially distinct receptors results in (C) a large fraction of bound indicator, but (D) low levels of free intracellular calcium. Panels show visualized model output at 4 times after release of transmitter. Insets show the simulated output expected from a fluorescence imaging experiment.

the receptors were bound (Fig. 6B). Note that these data only provide information on the number of open receptors at each point in time, but not whether this was due to a single-bound receptor that flickered rapidly between blocked and unblocked states, or a larger number of channels that opened independently at low probability, such that no two channels were open at the same time. When a receptor did open,  $\text{Ca}^{2+}$  entered the spine at the synapse, and diffused through the volume until it was extruded or buffered by CBPs or indicator. These brief epochs of  $\text{Ca}^{2+}$  influx, which continued for a long period due to the low dissociation rate of the NMDARs, led to efficient binding of  $\text{Ca}^{2+}$  by indicator due to its fast kinetics and high affinity (Fig. 6C), but did not result in a large increase in  $[\text{Ca}^{2+}]_i$  (Fig. 6D; c.f. Fig. 5).

Again, visualization of this simulation may clarify the difference between the action potential and EPSP-evoked signaling patterns. The observer is still inside the spine, but is now looking up toward the postsynaptic membrane. Closed/single-bound receptors are seen as ghostly, red structures on the spine ceiling. After binding glutamate and changing to their

open conformation, the receptors may be in either an open-blocked state (orange) or the conducting, open-unblocked state (red). The top edge of the spine apparatus is seen in the foreground, containing either  $\text{Ca}^{2+}$ -bound (black) or  $\text{Ca}^{2+}$ -free (gray) extrusion pumps. The representation of CBPs and indicator is the same as before.

Before any receptors opened (0 ms),  $[\text{Ca}^{2+}]_i$  was at low, resting levels. By 7.4 ms after release, five NMDARs were in the open state, although only one was unblocked (arrowhead). Influx through this receptor resulted in  $\text{Ca}^{2+}$  binding to CBPs and indicator near the receptor, before the channel reblocked. A short time later (14.3 ms) another channel was unblocked, allowing  $\text{Ca}^{2+}$  to enter a different region of the spine with low levels of buffer saturation. Still later (48.5 ms) a new channel has opened. By this time, a significant fraction of both CBP and indicator were  $\text{Ca}^{2+}$ -bound, resulting in the high fluorescent signal predicted by the inset and Fig. 6C. Thus, during an action potential,  $\text{Ca}^{2+}$  influx occurs through a small number of VDCCs that remained open for several milliseconds resulting in a volume of saturated buffer around



the channel. By contrast,  $Ca^{2+}$  entry during an EPSP was distributed in both time and space, resulting in efficient buffering of  $[Ca^{2+}]_i$  levels.

Our model does not yet allow for the complex signaling pathways, such as those necessary to model release of  $Ca^{2+}$  from intracellular stores. Although Emptage and colleagues report that NMDAR-mediated release of  $Ca^{2+}$  from stores underlies most of the  $Ca^{2+}$  signal following single, subthreshold EPSPs,<sup>(83)</sup> this result has not been reproduced.<sup>(38,43,84)</sup> Moreover, our simulations, which quantitatively match  $Ca^{2+}$  signaling profiles following an action potential, are able to account fully for the magnitude of the fluorescent  $Ca^{2+}$  signal during an EPSP using conservative estimates of NMDAR numbers and single-channel  $Ca^{2+}$  conductances, therefore suggesting that direct  $Ca^{2+}$  influx through NMDARs is sufficient to account for the observed increase in intracellular  $Ca^{2+}$ .

### Simulated neurochemistry

This preliminary work shows the important, but often overlooked, point that  $Ca^{2+}$  influx does not necessarily translate to  $[Ca^{2+}]_i$  in a simple and obvious manner. Instead,  $[Ca^{2+}]_i$  is an instantaneous cellular state determined by the concerted actions of  $Ca^{2+}$  influx, efflux and buffering. Indeed, STDP is probably not formally different from frequency-dependent selective induction of LTP and LTD. Instead, we suggest these be viewed as orthogonal dimensions of a multidimensional parameter space. For example, LTP induction by pre-

before-post correlated pairing depends on the frequency of pairing.<sup>(33,34)</sup> Similarly, the increase in  $[Ca^{2+}]_i$  in cerebellar Purkinje neurons following a train of action potentials is highly non-linear, with small increases in  $[Ca^{2+}]_i$  resulting from initial spikes but very large increases in  $[Ca^{2+}]_i$  towards the end of the train.<sup>(85)</sup> The authors show that the amount of  $Ca^{2+}$  influx following each spike is constant, and that the difference in  $[Ca^{2+}]_i$  is due to saturation of the buffering capacity. In a separate set of simulations, we have shown how the both  $[Ca^{2+}]_i$  and the activation of downstream  $Ca^{2+}$ -dependent proteins (CaM) are dependent on the complex interplay of the different processes regulating intracellular  $Ca^{2+}$  dynamics.<sup>(86)</sup>

Subthreshold EPSPs were presented 10 ms before somatic current injections to simulate  $Ca^{2+}$  dynamics under conditions that have been shown to produce a robust LTP. Five pairings at frequencies  $\leq 5$  Hz resulted in a large  $Ca^{2+}$  influx, but the  $Ca^{2+}$  was rapidly buffered by CBPs with different kinetics (Fig. 7A). The 200 ms interval between pairings was sufficiently long for most of  $Ca^{2+}$  to dissociate from the CBPs and be extruded from the cell before the arrival of the next pairing. This reloading of buffer prevented non-linear summation of  $[Ca^{2+}]_i$  (Fig. 7B) or activated, quaternary-bound CaM (CaM-4; Fig. 7C) in the spine. Although the amount of  $Ca^{2+}$  entering the cell was the same, at frequencies  $\geq 10$  Hz, CBPs were unable to offload  $Ca^{2+}$  ions bound from previous pairings, resulting in a saturation of the buffering capacity (Fig. 7D), such that increasing fractions of the  $Ca^{2+}$  entering

the cell on subsequent pairings would be unbuffered. This leads to highly cooperative increases in both  $[Ca^{2+}]_i$  (Fig. 7E) and CaM-4 (Fig. 7F). In general, CaM activation did not summate with pairings at frequencies up to 5 Hz, but increased non-linearly as pairing frequencies increased (Fig. 7G). Interestingly, 10 Hz is the lowest pairing frequency at which a small number of positively correlated pairings will reliably induce LTP.<sup>(33,34)</sup> If the frequency at which pairing becomes cooperative is due to saturation of the buffering capacity of the spine, then changing total buffering capacity should modulate this frequency dependence. Indeed, halving and doubling the CBP concentration resulted in increased and decreased frequency-dependence and CaM-4 levels, respectively. Again, very different intracellular  $[Ca^{2+}]_i$  profiles were induced without changing the amount of  $Ca^{2+}$  that entered the spine. Note that Sjöström and colleagues were able to induce LTP with low frequency pairing when the soma was mildly depolarized.<sup>(34)</sup> Although the chemical consequences at the synapse remain unknown, it is tempting to imagine that this depolarization leads to calcium spikes in dendritic branchlets,<sup>(87,88)</sup> such that the frequency-dependence of CaM activation is dramatically altered by an additional mode of  $Ca^{2+}$  entry.

#### Future direction

Clearly, this model does yet not explain the differences between the intracellular  $Ca^{2+}$  dynamics required for the induction of LTP and LTD, or the critical time-window of STDP. However, as illustrated above, these questions can only be answered using computational methods if the model incorporates the spatial, temporal and stochastic nature of intracellular signaling. Numerous studies have shown that  $Ca^{2+}$ -dependent reactions can sample  $Ca^{2+}$  in very local signaling domains, and recent ultrastructural and biochemical studies have shown exquisite spatial organization of signaling machinery at the synapse. It seems absurd to imagine that this organization is not critical in determining the dynamics and products of intracellular signaling transduction cascades. It is therefore equally absurd to imagine being able to really understand these important processes with an oversimplified model. We are therefore in the process of developing a model of a glutamatergic synapse of unprecedented biological detail and realism. Ultimately, this model will be implemented in a structure determined by three-dimensional serial reconstruction of electron tomographs of CA1 neuropil and will incorporate accurate estimates of the number, location and kinetic properties of all the appropriate synaptic signaling molecules. The completion of this project will require many years and active collaboration between different laboratories, and great effort. However, we contend that the answer to these, and many other outstanding biological questions, lie in the details, and it is therefore only by asking questions of sufficient detail, and by examining systems of sufficient complexity, that many of these answers can be found.

#### Conclusions

The Monte Carlo approach to modeling synapses presented here is still in its infancy. One of the important lessons that it has already taught us is the importance of knowing where  $Ca^{2+}$  enters the spine and its impact on the local microenvironment. This view contrasts with the impression from  $Ca^{2+}$  imaging experiments, of a well-mixed, homogenous milieu. Detailed simulations with MCell should allow us to refine our understanding of how  $Ca^{2+}$  interacts with elements of the PSD, and other subcellular compartments whose spatial organization appears to be crucial for the precise biochemical signaling required to achieve long-lasting changes in synaptic efficacy. In particular, we need to know more about the properties and locations of the calcium-binding proteins that regulate  $[Ca^{2+}]_i$  throughout the spine volume. No single discipline or set of techniques will be sufficient to provide a full understanding of the complexities of biological signaling. Instead, we expect that this will only be achieved with an open and active dialogue between disciplines; biophysically realistic simulations can provide a framework for building bridges between these disciplines and testing multidisciplinary hypotheses.

#### References

- Churchland PS, Sejnowski TJ. The computational brain. Cambridge, Mass: MIT Press; 1992.
- Bliss TV, Collingridge GL. A synaptic model of memory: long-term potentiation in the hippocampus. *Nature* 1993;361:31–39.
- Bliss TV, Lomo T. Long-lasting potentiation of synaptic transmission in the dentate area of the anaesthetized rabbit following stimulation of the perforant path. *J Physiol (Lond)* 1973;232:331–356.
- Sejnowski TJ. Statistical constraints on synaptic plasticity. *J Theor Biol* 1977;69:385–389.
- Bienenstock EL, Cooper LN, Munro PW. Theory for the development of neuron selectivity: orientation specificity and binocular interaction in visual cortex. *J Neurosci* 1982;2:32–48.
- Dunwiddie T, Lynch G. Long-term potentiation and depression of synaptic responses in the rat hippocampus: localization and frequency dependency. *J Physiol* 1978;276:353–367.
- Levy WB, Steward O. Temporal contiguity requirements for long-term associative potentiation/depression in the hippocampus. *Neuroscience* 1983;8:791–797.
- Dudek SM, Bear MF. Homosynaptic long-term depression in area CA1 of hippocampus and effects of N-methyl-D-aspartate receptor blockade. *Proc Natl Acad Sci USA* 1992;89:4363–4367.
- Malenka RC, Nicoll RA. Long-term potentiation—a decade of progress? *Science* 1999;285:1870–1874.
- Bekkers JM, Stevens CF. NMDA and non-NMDA receptors are colocalized at individual excitatory synapses in cultured rat hippocampus. *Nature* 1989;341:230–233.
- Isaac JT, Nicoll RA, Malenka RC. Evidence for silent synapses: implications for the expression of LTP. *Neuron* 1995;15:427–434.
- Takumi Y, Ramirez-Leon V, Laake P, Rinovik E, Ottersen OP. Different modes of expression of AMPA and NMDA receptors in hippocampal synapses. *Nat Neurosci* 1999;2:618–624.
- Artola A, Singer W. Long-term depression of excitatory synaptic transmission and its relationship to long-term potentiation. *Trends Neurosci* 1993;16:480–487.
- Lisman J. The CaM kinase II hypothesis for the storage of synaptic memory. *Trends Neurosci* 1994;17:406–412.

15. Lynch G, Larson J, Kelso S, Barrionuevo G, Schottler F. Intracellular injections of EGTA block induction of hippocampal long-term potentiation. *Nature* 1983;305:719–721.
16. Malenka RC, Kauer JA, Zucker RS, Nicoll RA. Postsynaptic calcium is sufficient for potentiation of hippocampal synaptic transmission. *Science* 1988;242:81–84.
17. Mulkey RM, Malenka RC. Mechanisms underlying induction of homosynaptic long-term depression in area CA1 of the hippocampus. *Neuron* 1992;9:967–975.
18. Malinow R, Schulman H, Tsien RW. Inhibition of postsynaptic PKC or CaMKII blocks induction but not expression of LTP. *Science* 1989;245:862–866.
19. Silva AJ, Wang Y, Paylor R, Wehner JM, Stevens CF, Tonegawa S. Alpha calcium/calmodulin kinase II mutant mice: deficient long-term potentiation and impaired spatial learning. *Cold Spring Harb Symp Quant Biol* 1992;57:527–539.
20. Mulkey RM, Herron CE, Malenka RC. An essential role for protein phosphatases in hippocampal long-term depression. *Science* 1993;261:1051–1055.
21. Mulkey RM, Endo S, Shenolikar S, Malenka RC. Involvement of a calcineurin/inhibitor-1 phosphatase cascade in hippocampal long-term depression. *Nature* 1994;369:486–488.
22. Cummings JA, Mulkey RM, Nicoll RA, Malenka RC. Ca<sup>2+</sup> signaling requirements for long-term depression in the hippocampus. *Neuron* 1996;16:825–833.
23. Nishiyama M, Hong K, Mikoshiba K, Poo MM, Kato K. Calcium stores regulate the polarity and input specificity of synaptic modification. *Nature* 2000;408:584–588.
24. Christie BR, Schexnayder LK, Johnston D. Contribution of voltage-gated Ca<sup>2+</sup> channels to homosynaptic long-term depression in the CA1 region in vitro. *J Neurophysiol* 1997;77:1651–1655.
25. Tang YP, Shimizu E, Dube GR, Rampon C, Kerchner GA, Zhuo M, Liu G, Tsien JZ. Genetic enhancement of learning and memory in mice. *Nature* 1999;401:63–69.
26. Malenka RC, Lanchester B, Zucker RS. Temporal limits on the rise in postsynaptic calcium required for the induction of long-term potentiation. *Neuron* 1992;9:121–128.
27. Neveu D, Zucker RS. Postsynaptic levels of [Ca<sup>2+</sup>]<sub>i</sub> needed to trigger LTD and LTP. *Neuron* 1996;16:619–629.
28. Yang SN, Tang YG, Zucker RS. Selective induction of LTP and LTD by postsynaptic [Ca<sup>2+</sup>]<sub>i</sub> elevation. *J Neurophysiol* 1999;81:781–787.
29. Wigstrom H, Gustafsson B, Huang YY, Abraham WC. Hippocampal long-term potentiation is induced by pairing single afferent volleys with intracellularly injected depolarizing current pulses. *Acta Physiol Scand* 1986;126:317–319.
30. Stuart GJ, Sakmann B. Active propagation of somatic action potentials into neocortical pyramidal cell dendrites. *Nature* 1994;367:69–72.
31. Debanne D, Gähwiler BH, Thompson SM. Long-term synaptic plasticity between pairs of individual CA3 pyramidal cells in rat hippocampal slice cultures. *J Physiol* 1998;507(Pt 1):237–247.
32. Bi GQ, Poo MM. Synaptic modifications in cultured hippocampal neurons: dependence on spike timing, synaptic strength, and postsynaptic cell type. *J Neurosci* 1998;18:10464–10472.
33. Markram H, Lubke J, Frotscher M, Sakmann B. Regulation of synaptic efficacy by coincidence of postsynaptic APs and EPSPs. *Science* 1997;275:213–215.
34. Sjostrom PJ, Turrigiano GG, Nelson SB. Rate, timing, and cooperativity jointly determine cortical synaptic plasticity. *Neuron* 2001;32:1149–1164.
35. Feldman DE. Timing-based LTP and LTD at vertical inputs to layer II/III pyramidal cells in rat barrel cortex. *Neuron* 2000;27:45–56.
36. Schuett S, Bonhoeffer T, Hubener M. Pairing-induced changes of orientation maps in cat visual cortex. *Neuron* 2001;32:325–337.
37. Yao H, Dan Y. Stimulus timing-dependent plasticity in cortical processing of orientation. *Neuron* 2001;32:315–323.
38. Zhang LI, Tao HW, Holt CE, Harris WA, Poo M. A critical window for cooperation and competition among developing retinotectal synapses. *Nature* 1998;395:37–44.
39. Yuste R, Denk W. Dendritic spines as basic functional units of neuronal integration. *Nature* 1995;375:682–684.
40. Magee JC, Johnston D. A synaptically controlled, associative signal for Hebbian plasticity in hippocampal neurons. *Science* 1997;275:209–213.
41. Koester HJ, Sakmann B. Calcium dynamics in single spines during coincident pre- and postsynaptic activity depend on relative timing of back-propagating action potentials and subthreshold excitatory postsynaptic potentials. *Proc Natl Acad Sci USA* 1998;95:9596–9601.
42. Yuste R, Majewska A, Cash SS, Denk W. Mechanisms of calcium influx into hippocampal spines: heterogeneity among spines, coincidence detection by NMDA receptors, and optical quantal analysis. *J Neurosci* 1999;19:1976–1987.
43. Sabatini BL, Oertner TG, Svoboda K. The life cycle of Ca<sup>2+</sup> ions in dendritic spines. *Neuron* 2002;33:439–452.
44. Denk W, Yuste R, Svoboda K, Tank DW. Imaging calcium dynamics in dendritic spines. *Curr Opin Neurobiol* 1996;6:372–378.
45. Zacharias DA, Baird GS, Tsien RY. Recent advances in technology for measuring and manipulating cell signals. *Curr Opin Neurobiol* 2000;10:416–421.
46. Yuste R, Majewska A, Holthoff K. From form to function: calcium compartmentalization in dendritic spines. *Nat Neurosci* 2000;3:653–659.
47. Nimchinsky EA, Sabatini BL, Svoboda K. Structure and function of dendritic spines. *Annu Rev Physiol* 2002;64:313–353.
48. Mainen ZF, Malinow R, Svoboda K. Synaptic calcium transients in single spines indicate that NMDA receptors are not saturated. *Nature* 1999;399:151–155.
49. Sabatini BL, Svoboda K. Analysis of calcium channels in single spines using optical fluctuation analysis. *Nature* 2000;408:589–593.
50. Llinas R, Sugimori M, Silver RB. Microdomains of high calcium concentration in a presynaptic terminal. *Science* 1992;256:677–679.
51. Shaywitz AJ, Greenberg ME. CREB: a stimulus-induced transcription factor activated by a diverse array of extracellular signals. *Annu Rev Biochem* 1999;68:821–861.
52. Deisseroth K, Bito H, Tsien RW. Signaling from synapse to nucleus: postsynaptic CREB phosphorylation during multiple forms of hippocampal synaptic plasticity. *Neuron* 1996;16:89–101.
53. Dolmetsch RE, Pajvani U, Fife K, Spotts JM, Greenberg ME. Signaling to the nucleus by an L-type calcium channel-calmodulin complex through the MAP kinase pathway. *Science* 2001;294:333–339.
54. Hardingham GE, Arnold FJ, Bading H. A calcium microdomain near NMDA receptors: on switch for ERK-dependent synapse-to-nucleus communication. *Nat Neurosci* 2001;4:565–566.
55. Takasu MA, Dalva MB, Zigmund RE, Greenberg ME. Modulation of NMDA receptor-dependent calcium influx and gene expression through EphB receptors. *Science* 2002;295:491–495.
56. Walikonis RS, Jensen ON, Mann M, Provance DW Jr, Mercer JA, Kennedy MB. Identification of proteins in the postsynaptic density fraction by mass spectrometry. *J Neurosci* 2000;20:4069–4080.
57. Husi H, Ward MA, Choudhary JS, Blackstock WP, Grant SG. Proteomic analysis of NMDA receptor-adhesion protein signaling complexes. *Nat Neurosci* 2000;3:661–669.
58. Valtschanoff JG, Weinberg RJ. Laminar organization of the NMDA receptor complex within the postsynaptic density. *J Neurosci* 2001;21:1211–1217.
59. Sheng M, Lee SH. Growth of the NMDA receptor industrial complex. *Nat Neurosci* 2000;3:633–635.
60. Kennedy MB. Signal-processing machines at the postsynaptic density. *Science* 2000;290:750–754.
61. Hayashi Y, Shi SH, Esteban JA, Piccini A, Poncer JC, Malinow R. Driving AMPA receptors into synapses by LTP and CaMKII: requirement for GluR1 and PDZ domain interaction. *Science* 2000;287:2262–2267.
62. Wu J, Wang Y, Rowan MJ, Anwyl R. Evidence for involvement of the neuronal isoform of nitric oxide synthase during induction of long-term potentiation and long-term depression in the rat dentate gyrus in vitro. *Neuroscience* 1997;78:393–398.
63. English JD, Sweatt JD. A requirement for the mitogen-activated protein kinase cascade in hippocampal long term potentiation. *J Biol Chem* 1997;272:19103–19106.
64. Cho KO, Hunt CA, Kennedy MB. The rat brain postsynaptic density fraction contains a homolog of the Drosophila discs-large tumor suppressor protein. *Neuron* 1992;9:929–942.

65. Kornau HC, Seeburg PH, Kennedy MB. Interaction of ion channels and receptors with PDZ domain proteins. *Curr Opin Neurobiol* 1997;7:368–373.
66. Kornau HC, Schenker LT, Kennedy MB, Seeburg PH. Domain interaction between NMDA receptor subunits and the postsynaptic density protein PSD-95. *Science* 1995;269:1737–1740.
67. Niethammer M, Kim E, Sheng M. Interaction between the C terminus of NMDA receptor subunits and multiple members of the PSD-95 family of membrane-associated guanylate kinases. *J Neurosci* 1996;16:2157–2163.
68. Kim E, Cho KO, Rothschild A, Sheng M. Heteromultimerization and NMDA receptor-clustering activity of Chapsyn-110, a member of the PSD-95 family of proteins. *Neuron* 1996;17:103–113.
69. Tejedor FJ, Bokhari A, Rogero O, Gorczyca M, Zhang J, Kim E, Sheng M, Budnik V. Essential role for dlx in synaptic clustering of Shaker K<sup>+</sup> channels in vivo. *J Neurosci* 1997;17:152–159.
70. Migaud M, Charlesworth P, Dempster M, Webster LC, Watabe AM, Makhinson M, He Y, Ramsay MF, Morris RG, Morrison JH, O'Dell TJ, Grant SG. Enhanced long-term potentiation and impaired learning in mice with mutant postsynaptic density-95 protein. *Nature* 1998;396:433–439.
71. Malenka RC. Synaptic plasticity in the hippocampus: LTP and LTD. *Cell* 1994;78:535–538.
72. Lee HK, Barbarosie M, Kameyama K, Bear MF, Huganir RL. Regulation of distinct AMPA receptor phosphorylation sites during bidirectional synaptic plasticity. *Nature* 2000;405:955–959.
73. Sanes JR, Lichtman JW. Can molecules explain long-term potentiation? *Nat Neurosci* 1999;2:597–604.
74. Stiles JR, Bartol TM Jr. Monte Carlo methods for simulating realistic synaptic microphysiology. In: de Schutter E, editor. *Computational Neuroscience: Realistic Modeling for Experimentalists* Boca Raton CRC Press; 2001. 87–127.
75. Stiles JR, Bartol TM Jr, Salpeter EE, Salpeter MM, Sejnowski TJ. Synaptic variability: new insights from reconstructions and Monte Carlo simulations with MCell. In: Cowan WM, Sudhof TC, Stevens CF, editors. *Synapses* Baltimore Johns Hopkins University Press; 2001. 681–731.
76. Bartol TM Jr, Land BR, Salpeter EE, Salpeter MM. Monte Carlo simulation of miniature endplate current generation in the vertebrate neuromuscular junction. *Biophys J* 1991;59:1290–1307.
77. Anglister L, Stiles JR, Salpeter MM. Acetylcholinesterase density and turnover number at frog neuromuscular junctions, with modeling of their role in synaptic function. *Neuron* 1994;12:783–794.
78. Stiles JR, Van Helden D, Bartol TM Jr, Salpeter EE, Salpeter MM. Miniature endplate current rise times less than 100 microseconds from improved dual recordings can be modeled with passive acetylcholine diffusion from a synaptic vesicle. *Proc Natl Acad Sci USA* 1996;93:5747–5752.
79. Faber DS, Young WS, Legendre P, Korn H. Intrinsic quantal variability due to stochastic properties of receptor-transmitter interactions. *Science* 1992;258:1494–1498.
80. Wahl LM, Pouzat C, Stratford KJ. Monte Carlo simulation of fast excitatory synaptic transmission at a hippocampal synapse. *J Neurophysiol* 1996;75:597–608.
81. Franks KM, Bartol TM Jr, Sejnowski TJ. A Monte Carlo model reveals independent signaling at central glutamatergic synapses. *Biophys J* 2002;
82. Hines ML, Carnevale NT. The NEURON simulation environment. *Neural Comput* 1997;9:1179–1209.
83. Emptage N, Bliss TV, Fine A. Single synaptic events evoke NMDA receptor-mediated release of calcium from internal stores in hippocampal dendritic spines. *Neuron* 1999;22:115–124.
84. Kovalchuk Y, Eilers J, Lisman J, Konnerth A. NMDA receptor-mediated subthreshold Ca<sup>2+</sup> signals in spines of hippocampal neurons. *J Neurosci* 2000;20:1791–1799.
85. Maeda H, Ellis-Davies GC, Ito K, Miyashita Y, Kasai H. Supralinear Ca<sup>2+</sup> signaling by cooperative and mobile Ca<sup>2+</sup> buffering in Purkinje neurons. *Neuron* 1999;24:989–1002.
86. Franks KM, Bartol TM Jr, Sejnowski TJ. An MCell model of calcium dynamics and frequency-dependence of calmodulin activation in dendritic spines. *Neurocomput* 2001;38–40:9–16.
87. Schiller J, Major G, Koester HJ, Schiller Y. NMDA spikes in basal dendrites of cortical pyramidal neurons. *Nature* 2000;404:285–289.
88. Wei DS, Mei YA, Bagal A, Kao JP, Thompson SM, Tang CM. Compartmentalized and binary behavior of terminal dendrites in hippocampal pyramidal neurons. *Science* 2001;293:2272–2275.
89. Svoboda K, Tank DW, Denk W. Direct measurement of coupling between dendritic spines and shafts. *Science* 1996;272:716–719.
90. Majewska A, Tashiro A, Yuste R. Regulation of spine calcium dynamics by rapid spine motility. *J Neurosci* 2000;20:8262–8268.